



Introduction

NOAO is actively developing a broader “System” of telescope access to satisfy observers’ needs for a diverse set of facilities and capabilities. The science highlights chosen for this *Newsletter* issue illustrate that kind of diversity:

- Søren Meibom’s article on measuring stellar ages was made possible by a unique service observing opportunity at the WIYN 0.9-meter telescope, combined with spectroscopy from the WIYN 3.5-meter telescope;
- Howard Bond’s work uses such diverse facilities as an amateur 12-inch telescope, the SMARTS Consortium 1.3-meter and 1.5-meter telescopes, and the Hubble Space Telescope;
- David Yong needed the Phoenix infrared spectrograph, originally deployed at the NOAO 4-meter telescopes, but now at Gemini;
- Laura Magrini’s study was enabled through the Telescope System Instrumentation Program access to the MMT; and
- Todd Boroson’s and Tod Lauer’s analysis demonstrates the power of digging through large data sets from the Sloan Digital Sky Survey, representing a forward look to the kind of algorithms that will become common in the era of much larger data sets such as those that will be produced by the Large Synoptic Survey Telescope.

– George Jacoby

Stellar Ages from Stellar Rotation

Søren Meibom (Harvard-Smithsonian Center for Astrophysics)

Introduction

As part of the WIYN Open Cluster Study (WOCS), my collaborators R. Mathieu (University of Wisconsin), K. Stassun (Vanderbilt University), and I have obtained extensive time-series radial-velocity observations and highly precise time-series photometric observations of late-type stars in the 150 Myr and 200 Myr open clusters M35 (NGC 2168) and M34 (NGC 1039). When combined, these data sets allow us to distinguish cluster membership and binarity in the clusters, and to derive rotation periods. The collection of the survey data was made possible with generous telescope time allocations through NOAO and University of Wisconsin–Madison; the photometric program relied heavily on queue-scheduled observations taken by a long list of WIYN 0.9-m telescope observers (the author gives a big thank you to them all).

Our objective was to learn about the rotational evolution of single stars and stars in close binaries, and how this evolution depends on the stellar mass in clusters with different ages. Stellar rotation, and its dependence on stellar age and mass (color), has recently come to the fore as a distance-independent indicator of age (“gyrochronology;” Barnes 2003a, 2007). However, our ability to determine stellar ages

from measurements of stellar rotation hinges on how well we can measure the dependence of rotation on age for stars of different masses. For that purpose, rotation periods for stars in open clusters are essential.

Knowing stellar ages is fundamental to understanding the time-evolution of astronomical phenomena related to stars and their companions. Accordingly, over the past decades much work has been focused on identifying the properties of a star that best reveal its age. For coeval populations of stars in clusters, the most reliable ages are determined by fitting model isochrones to single cluster members in the color-magnitude diagram. However, for the vast majority of stars not in clusters (e.g., unevolved, late-type field stars), ages determined using the isochrone method are highly uncertain because the primary age indicators are nearly constant throughout their main-sequence lifetimes, and because their distances and thus luminosities are poorly known. Therefore, finding a distance-independent property of individual stars that can act as a reliable determinant of their ages is extremely valuable.

Stellar rotation has been demonstrated to be a promising and distance-independent indica-

tor of age (Skumanich 1972; Kawaler 1989; Barnes 2003a, 2007). Skumanich (1972) first established stellar rotation as an astronomical clock by relating the average projected rotation velocity in young open clusters to their ages. The Skumanich relation is limited in mass to early G dwarfs and suffers from the ambiguity of the $v \sin(i)$ data. Furthermore, for ages beyond that of the Hyades cluster (625 Myr), the Skumanich relationship is constrained only by a single G2 dwarf—the Sun.

Modern photometric time-series surveys in young, open clusters can provide precisely measured stellar rotation periods (free of the $\sin(i)$ ambiguity) for F, G, K, and M dwarfs. Based on such new data and emerging empirical relationships between stellar rotation, color, and age, a method was proposed by Barnes (2003a) to derive ages for late-type dwarfs from observations of their colors and rotation periods alone. (See Barnes 2003a for a description of the method of gyrochronology.)

The Key Role of Open Clusters

Open clusters are coeval populations of stars with a range of masses and well-determined ages, and, therefore, fulfill a critically important role in calibrating the relations between stellar age, rotation, and color. Indeed, open

continued

Stellar Ages from Stellar Rotation continued

clusters can define a surface in the three-dimensional space of stellar rotation period, color, and age, from which the latter can be determined from measurements of the former two (see figure 1 to the right).

This inherent quality of open clusters can only be fully exploited if precise stellar rotation periods (free of the $\sin(i)$ ambiguity) are measured for cluster members. Accordingly, the time baseline and frequency of time-series photometric observations must be long enough and high enough, respectively, to avoid a bias against detecting periods of more slowly rotating stars, and to avoid detection of false rotation periods due to aliases and a strong “window-function” in the data. Furthermore, measured rotation periods must be considered in combination with cluster membership and multiplicity data. Removing non-members and stars in close binaries affected by tidal synchronization improves the definition of the relationship between rotation period and color at the age of the cluster. Also, identification of single cluster members improves cluster age determinations from isochrone fitting. Our new results for the open clusters M35 and M34 shown in figure 2 reflect the powerful combination of decade-long, time-series spectroscopy for cluster membership and time-series photometry over five months for stellar rotation periods.

The Color-Period Diagram

Figure 2 shows the rotational periods for members in M35 and M34 plotted against their de-reddened (B-V) colors. The coeval stars fall along two well-defined sequences representing two different rotational states. One sequence displays a clear correlation between rotation period and color, and forms a diagonal band of stars whose periods are increasing with increasing color index (decreasing mass). The second sequence consists of rapidly rotating stars and shows little mass dependence. A small subset of stars is distributed between the two sequences. The distribution of stars in the color-period diagrams suggests that the rotational evolution is slow where we see the sequences and fast in the gap between them. Other areas of the color-period plane are either unlikely or “forbidden.”

The Dependence of Stellar Rotation Period on Color

For our purpose of determining the dependence of stellar rotation on stellar color, we can focus on the diagonal sequence of more

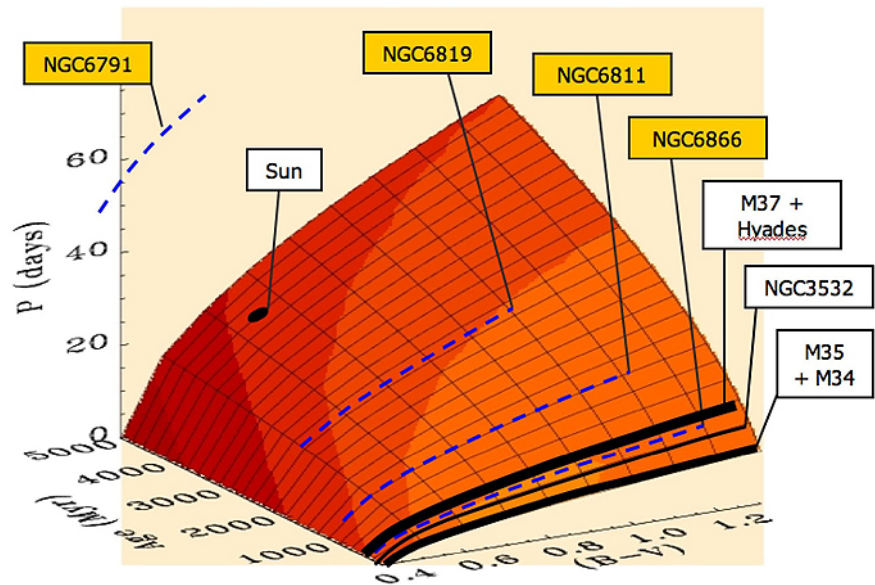


Figure 1: A schematic of the (presumed) empirical surface in the three-dimensional parameter space of stellar age (Myr), color (mass), and rotation period. The surface is currently defined only by stars in young open clusters (black solid lines) and by the Sun (black dot). The dashed blue lines mark the ages and approximate color ranges of FGK dwarfs in the four open clusters within the Kepler field.

slowly rotating stars in figure 2. We can do so because surveys for stellar rotation in the older clusters M37 (550 Myr) and the Hyades (625 Myr) show that F, G, and K dwarfs spin down over a few hundred million years and converge onto this sequence.

Barnes (2003a, 2007) refers to the diagonal sequence as the Interface (I) sequence and proposes a function to represent it. From the method of gyrochronology, the functional

dependence between stellar color and rotation period will directly affect the derived ages and will, if not accurately determined, introduce a systematic error. It is therefore important to constrain and test the color-rotation relation for stars on the I sequence as new data of sufficiently high quality become available. In Meibom et al. (2009), we fit the function suggested by Barnes (2007) to the I sequence stars in M35, leaving all coefficients as free parameters. We get nearly the same

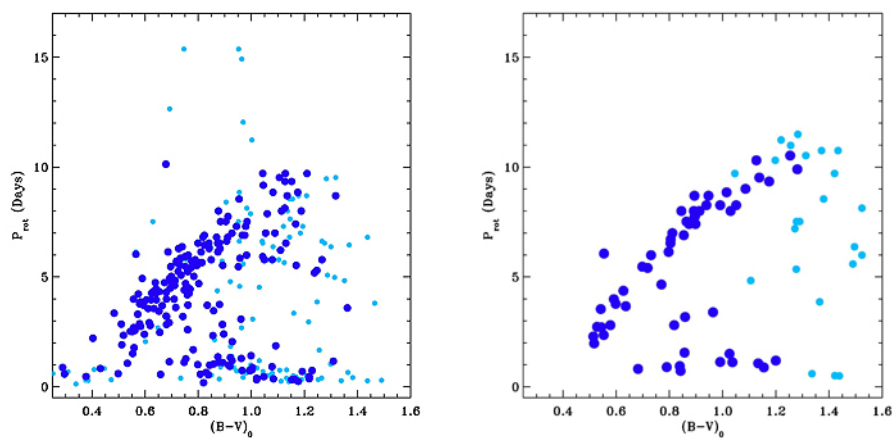


Figure 2: The distribution of stellar rotation periods with (B-V) color index for 310 members of the open cluster M35 (left) and 79 members of the open cluster M34 (right). Dark blue (black) plotting symbols are used for radial-velocity members and light blue (grey) for photometric members.

continued

Stellar Ages from Stellar Rotation continued

coefficients, but by leaving the translational term free, we find a value of 0.47, which corresponds to the approximate (B-V) color for F-type stars at the transition from a radiative to a convective envelope. This transition is also associated with the onset of effective magnetic-wind breaking (Schatzman 1962) and is known as the break in the Kraft curve (Kraft 1967). The value of 0.47 suggests that for M35 the high-mass end of the I sequence begins at the break in the Kraft curve. The I sequence in M34 is particularly well-defined and will be used to further constrain the dependence between rotation and color in a forthcoming paper (Meibom et al. 2009, in preparation).

The Dependence of Stellar Rotation Period on Age

With well-defined color-rotation relations (I sequences) for clusters of different ages, we are able to constrain the dependence of stellar rotation on age for stars of different masses. By comparing the rotation periods for F-, G-, and K-type I-sequence dwarfs at different ages, we can make a direct test of the Skumanich relationship for early G dwarfs and for dwarfs of higher and lower masses.


When this test is applied to G and K dwarfs on the I sequences in M35 and the Hyades, the Skumanich time-dependence can be shown to account for the evolution in rota-

tion periods of G dwarfs in these clusters. However, the time-dependence for spin-down of K dwarfs is slower than the Skumanich relation (Meibom 2009). In a more in-depth analysis, preliminary results of a comparison of the mean rotation periods of late-F, G, early-K, and late-K I-sequence dwarfs in M35, M34, NGC 3532 (Barnes 2003a; 300 Myr), M37, and the Hyades, show that age is consistent with Skumanich spin-down for the late-F and G dwarfs, but the K dwarfs spin down significantly slower (Meibom et al. 2009, in preparation).

The Kepler Mission—A Special Opportunity

At the present time, the Hyades represents the oldest coeval population of stars with measured rotation periods. Measurements of rotation periods for older, late-type dwarfs are needed to properly constrain the dependence of stellar rotation on age and mass, and to calibrate the technique of gyrochronology. Figure 1 shows a schematic of the surface in the three-dimensional space of rotation, color, and age. At the present time, this surface is defined solely by color-period data in young clusters and for the Sun. The solid black curves represent the ages and color-ranges of FGK dwarfs in M35, M34, NGC 3532, M37, and the Hyades. The color and age of the Sun is marked as a solid dot. The figure demonstrates clearly the need

for observations of stellar rotation periods beyond the age of the Hyades.

The lack of periods for older stars (with the exception of the Sun) reflects the challenging task of measuring from the ground the photometric variability for slowly rotating stars with ages of 1 Gyr or more. However, the Kepler space telescope (scheduled for a 2009 launch) will provide photometric measurements with a precision, cadence, and duration sufficient to measure stellar rotation periods from brightness modulations for stars that are even older than the Sun. Four open clusters are located within the Kepler target region: NGC 6866 (0.5 Gyr), NGC 6811 (1 Gyr), NGC 6819 (2.5 Gyr), and NGC 6791 (~10 Gyr). With Kepler, we have a unique opportunity to extend the age-rotation-color relationships beyond the age of the Hyades and the Sun. 

REFERENCES

- Barnes 2003, ApJ, 586, 464
- Barnes 2007, ApJ, 669, 1167
- Kawaler 1989, ApJL, 343, L65
- Kraft 1967, ApJ, 150, 551
- Meibom, Mathieu, & Stassun 2009, Accepted to ApJ, \eprint{0805.1040}
- Schatzman 1962, Annales d'Astrophysique, 25, 18
- Skumanich 1972, ApJ, 171, 565

Luminous Transients in Nearby Galaxies

*Howard E. Bond, Luigi R. Bedin, Alceste Z. Bonanos (STScI),
Roberta M. Humphreys (University of Minnesota), Berto Monard (Bronberg Observatory),
Jose L. Prieto (Ohio State University) & Frederick M. Walter (Stony Brook University)*

The outbursts of classical novae (CNe) and supernovae (SNe) have been known to astronomers for decades. More recently, stellar eruptions with luminosities intermediate between CNe and SNe and outburst time scales of a few months are being discovered in increasing numbers. This is the result of surveys for transients by professional and amateur observers that are reaching greater depths and sky coverage. These new types of outbursts are posing new challenges to our understanding of late stages of stellar evolution.

The term “supernova impostors” was introduced by Van Dyk et al. (2000) following the outburst of SN 1997bs. Although superficially resembling a narrow-lined Type IIIn SN in spectrum and light curve, the SN 1997bs event reached an absolute magnitude at maximum more than 3 mag fainter than a typical core-collapse SN. Van Dyk et al. argued that SN 1997bs was instead a “superoutburst” of a mas-

sive, luminous blue variable (LBV), analogous to those experienced historically by the Galactic objects P Cygni and eta Carinae.

The recent outburst of SN 2008S, which had a SN IIIn spectrum but only reached an absolute magnitude of -14, has been discussed by Thompson et al. (2008) and Smith et al. (2008). Remarkably, Prieto et al. (2008) used archival Spitzer images to show that the progenitor of SN 2008S was a luminous infrared star, deeply enshrouded in circumstellar dust, and thus dissimilar to the LBVs P Cyg and eta Car.

V838 Monocerotis (V838 Mon) belongs to an apparently separate class of transients also lying in the CN-SN gap. Its 2002 eruption, discovered by an amateur, illuminated a spectacular light echo (Bond et al. 2003) that yielded a geometric distance to the star (Sparks et al. 2008). Unlike a CN, V838 Mon became progressively redder during

continued

Luminous Transients in Nearby Galaxies continued

its outburst. Its light curve was very different from that of a SN, CN, or LBV eruption, showing a series of four maxima separated by about a month each. It has been proposed that the outburst of V838 Mon was due to a stellar merger or collision. Possible extragalactic analogs of V838 Mon include the 1988 outburst of a luminous red object in the Andromeda galaxy—denoted the M31 red variable, or “M31 RV” (Bond & Siegel 2006)—and a luminous red transient in the Virgo galaxy M85 in 2006 (Kulkarni et al. 2007).

We describe observations of a new, luminous transient discovered in May 2008 in the nearby Southern Hemisphere galaxy NGC 300. Our results serve to illustrate the broad wavelength coverage now available to ground- and space-based observatories, the contributions of amateur astronomers, and the power of the quick response and synoptic capabilities of the telescopes in the Small and Medium Aperture Research Telescope System (SMARTS) at NOAO’s Cerro Tololo Inter-American Observatory (CTIO).

The NGC 300 optical transient (NGC 300 OT) was discovered by the amateur member of our team, Berto Monard, during his SN search program at his private 0.3-m observatory in South Africa. NGC 300 is a spiral galaxy in the Sculptor Group, lying just outside the Local Group at a distance of 1.9 Mpc. A normal SN in this galaxy would peak brighter than 10th mag. At discovery, however, the NGC 300 OT was only at 14.3 mag.

Because of our interest in luminous transients, we immediately began a program of photometric and spectroscopic monitoring of the NGC 300 OT, using the 1.3-m and 1.5-m telescopes at CTIO operated by the SMARTS consortium (www.astro.yale.edu/smarts).

The Chilean service observers employed by SMARTS can respond very quickly to target-of-opportunity requests. Thus, within a day of its announcement on the Central Bureau for Astronomical Telegrams (CBAT) Unconfirmed Observations Page, we obtained the first spectrum (Bond et al. 2008) of the NGC 300 OT, shown at the top of figure 1. This remarkable spectrum exhibits strong emission at H α , H β , and the Ca II triplet at 8542-8498-8662 Å. Most surprisingly, it has strong emission at the unusual forbidden [Ca II] doublet at 7291-7323 Å. These are superposed on an F-type supergiant absorption spectrum. Overall, the low-excitation spectrum is indicative of an optically thick wind or envelope, slowly expanding away from the site of the outburst. We continued the spectroscopic monitoring throughout 2008; by August, as shown in figure 1, the continuum had faded but the emission lines continued to be strong.

Since the spectrum of the NGC 300 OT was somewhat similar to that of V838 Mon at a comparable stage in its outburst, we also began a program of photometric monitoring, in anticipation of detecting periodic spikes like those of V838 Mon. These observations are being done with the SMARTS 1.3-m telescope and its ANDICAM camera, which obtains simultaneous optical and near-infrared (IR) images using CCD and IR detectors. Figure 2 shows the light curve up to the present. As it turned out, the light curve of the NGC 300 OT did not show any spikes, but instead declined smoothly, superficially resembling a SN but at a considerably lower luminosity. The rise to maximum was not well covered, but was clearly more rapid than the subsequent decline. The NGC 300 OT has become steadily redder as it fades.

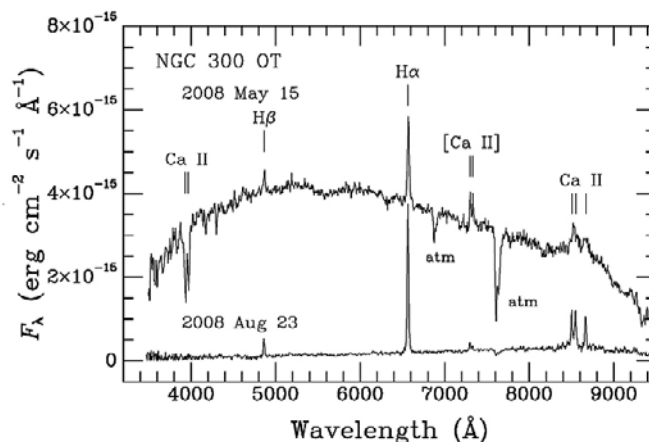


Figure 1: Low-resolution SMARTS 1.5-m spectra of the NGC 300 OT on 15 May and 23 August 2008. In the May observation, note strong emission lines of H, Ca II, and [Ca II] superposed on an F-type absorption spectrum. By August, the continuum had faded dramatically and the spectrum was dominated by emission lines.

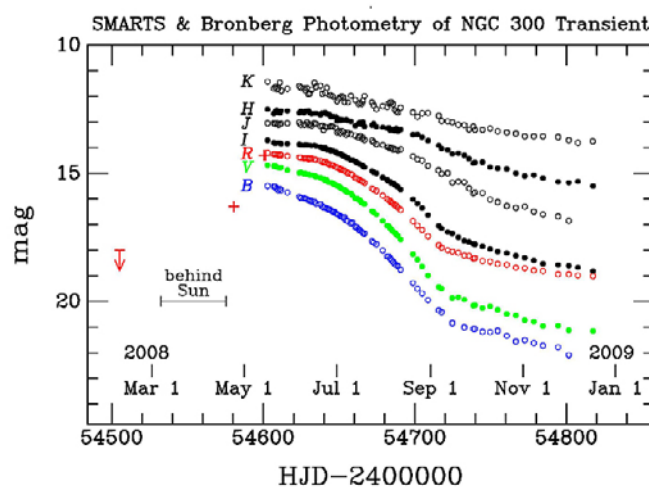


Figure 2: BVRIJK light curve of the NGC 300 OT. SMARTS 1.3-m telescope data are shown as open and filled circles. Monard’s Bronberg 0.3-m discovery observations and a pre-discovery detection are shown as crosses, and the downward arrow on the left shows Monard’s upper limit in February 2008.

There are deep archival Hubble Space Telescope (HST) images of NGC 300, taken before the outburst. The HST images reveal an extremely rich field of resolved stars at the OT site, lying in a spiral arm of NGC 300. In order to localize the OT with high astrometric precision, we obtained new HST images of the outburst site with the WFPC2 camera in June 2008. To our surprise, there is no progenitor object detected in the archival HST images to a limit of V magnitude 28.5.

However, a luminous star *is* present at the OT location in archival Spitzer images obtained in 2003 and 2007, as first reported by Prieto (2008). This source is detected throughout the mid-IR, from 3.6 to 24 microns, with a black-body fit giving a temperature of 350 K, an enormous radius of 300 AU, and a luminosity of $5.5 \times 10^4 L_{\odot}$.

continued

Luminous Transients in Nearby Galaxies continued

These observations are consistent with the progenitor being an evolved supergiant of about 10–15 M_{\odot} , heavily enshrouded in a surrounding dust shell that blocked the optical light and reprocessed it to the mid-IR. This optically hidden star then underwent a sudden outburst that evaporated most of the surrounding dust. The exact nature of the outburst, however, remains unknown: it may have been some type of as-yet unexplained failed SN, a photospheric eruption of an uncertain origin, or, as suggested by Berger et al. (2009), a violent binary interaction.

This new type of stellar eruption may not be uncommon, as illustrated by two very similar events (SN 2008S and NGC 300) occurring in the same year. The forthcoming synoptic surveys, including Pan-STARRS and LSST, are likely to reveal many new examples. \bullet

Details of our observations are given in Bond et al. (2009).

REFERENCES

Berger, E., et al. 2009, arXiv:0901.0710
 Bond, H. E., et al. 2003, *Nature*, 422, 405
 Bond, H. E., & Siegel, M. H. 2006, *AJ*, 131, 984
 Bond, H. E., Walter, F. M., & Velasquez, J. 2008, *IAU Circ*, 8946, 2
 Bond, H. E., et al. 2009, arXiv:0901.0198
 Kulkarni, S. R., et al. 2007, *Nature*, 447, 458
 Prieto, J. L. 2008, *The Astronomer's Telegram*, 1550, 1
 Smith, N., et al. 2008, arXiv:0811.3929
 Sparks, W. B., et al. 2008, *AJ*, 135, 605
 Thompson, T. A., et al. 2008, arXiv:0809.0510
 Van Dyk, S. D., et al. 2000, *PASP*, 112, 1532

Chemical Abundances in the Tidally Disrupted Globular Cluster NGC 6712

*David Yong (ANU), Jorge Meléndez (Centro de Astrofísica de Universidade do Porto),
 Katia Cunha (NOAO), Amanda Karakas, John Norris (ANU) & Verne Smith (NOAO)*

Globular clusters are the oldest Galactic objects for which reliable ages can be obtained and have long been regarded to be the first bound systems to have formed in the protogalactic era. As such, they have witnessed the subsequent formation and evolution of our Galaxy. However, were globular clusters innocent bystanders to the chaotic hierarchical assembly of our Galaxy, or were they active, albeit presumably minor, participants? After all, some contend that all field stars were born in clusters.

Spectacular tidal tails associated with the globular clusters Palomar 5 and NGC 5466 have been revealed by the Sloan Digital Sky Survey. Therefore, these tidally disrupted clusters are currently contributing stars to the disk and halo. For both clusters, additional evidence for tidal stripping comes from their flat mass functions, which reveal significant depletions of low-mass stars presumably stripped by the Galactic tidal field.

Detailed chemical abundances place strong constraints upon the fraction of field stars that may have been born in globular clusters and/or the types of globular clusters that may populate the disk and halo. Every well-studied Galactic globular cluster, including Palomar 5 (Smith et al. 2002), has large star-to-star abundance variations for the light elements from C to Al. Within a given cluster, the abundances of C and O are low when N is high, O and Na are anticorrelated, as are Mg and Al. While hydrogen burning at high temperatures can explain these abundance patterns, the source of the nucleosynthesis and the nature of the pollution mechanism remain unknown. Nevertheless, these abundance patterns have yet to be found in field stars. The discovery of a tidally disrupted globular cluster in which there are no light element abundance variations would open the possibility that clusters could have played a considerable role in building up our Galaxy.

NGC 6712 is the only globular cluster whose mass function actually decreases with decreasing mass (Paresce & De Marchi 2000). With an

orbit penetrating deep into the bulge, tidal forces have stripped away a substantial fraction of low-mass stars. Due to the high reddening, chemical abundances for this cluster are best obtained at near infrared wavelengths. In this study, we obtained high-resolution H-band and K-band spectra using the Phoenix spectrograph on Gemini-South (see figure 1). From these spectra, we measured the relative abundances of C, N, O, F, Na, and Fe (Yong et al. 2008).

We assume that observing cluster giants is equivalent to observing giants in the tidal tails, thus, we can probe the compositions of tidally stripped stars. Even within our small sample of seven bright giant stars, we found large abundance variations for C, N, O, F, and Na (see figure 2). Such patterns are not found in field stars, therefore, clusters like NGC 6712 and Palomar 5 cannot provide many field stars, and/

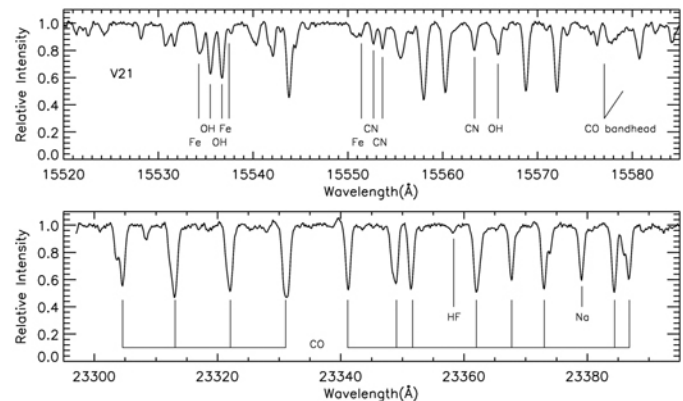


Figure 1: Spectra of NGC 6712 V21 for the two wavelength regions. Lines used in the abundance analysis are indicated.

continued

Chemical Abundances in NGC 6712 continued

or field stars do not form in environments with chemical enrichment histories like those of NGC 6712 and Palomar 5.

NGC 6712 is only the second cluster in which F has been observed in more than two stars and both clusters show F abundance variations, which may be produced in AGB stars with masses $> 5 M_{\odot}$ (Smith et al. 2005). The fluorine abundances in globular clusters are considerably lower than in field and bulge stars at the same metallicity (see figure 3), which highlights additional chemical differences between the field and cluster environment. In the context of trying to identify the source of the light element abundance variations, our study has reinforced the importance of accounting for F (this element shows the largest abundance variation amplitude of all elements measured in this cluster).

Finally, the chemical abundances measured in this cluster offer the intriguing prospect of allowing us to estimate its initial mass, and therefore, the fraction of mass lost through tidal stripping. Carretta (2006) found a correlation between the amplitude of the abundance variations and the absolute magnitude. Based on the abundance amplitudes, we tentatively confirm the calculations by Takahashi & Portegies Zwart (2000), which indicate that NGC 6712 was once one of the most massive clusters to have formed in our Galaxy.

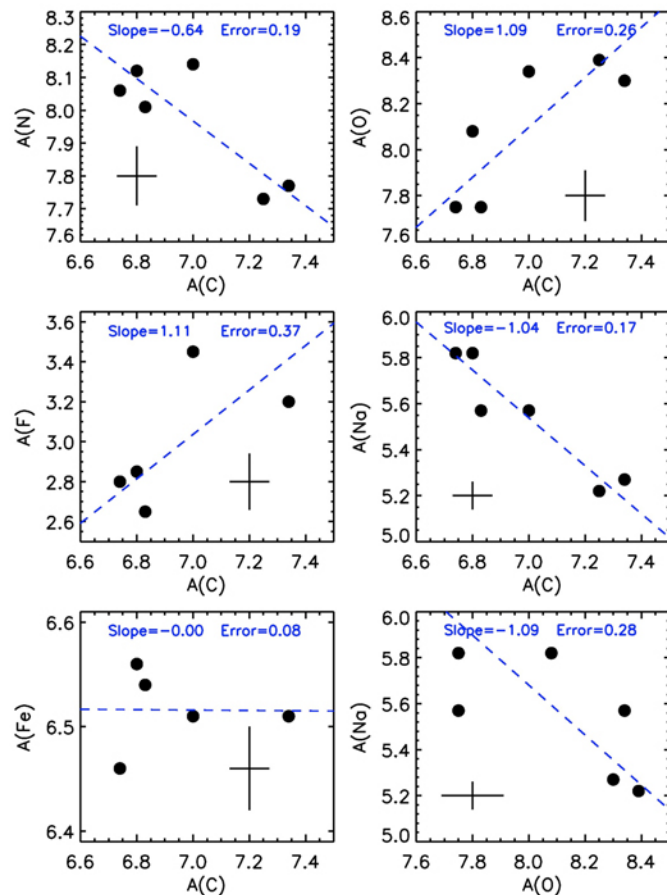


Figure 2: Elemental abundances $A(X)$ vs. $A(C)$ as well as $A(Na)$ vs. $A(O)$ (bottom right panel). A representative error bar is shown. The dashed line is the linear least-squares fit to the data (slope and associated error are included).

Of great interest would be the chemical analysis of additional globular clusters that show evidence for tidal disruption to search for a cluster in which there are no light element abundance variations. Equally important would be to expand the search for field stars that exhibit the “globular cluster light element abundance patterns.” These endeavors will enhance our understanding of the formation and evolution of our Galaxy.

I wish to thank my long-time collaborators David Lambert and Frank Grundahl. ☾

REFERENCES

Carretta 2006, AJ, 131, 1766
 Cunha et al. 2003, AJ, 126, 1305
 Cunha & Smith 2005, ApJ, 626, 425
 Cunha et al. 2008, ApJ, 679, L17
 Paresce & De Marchi 2000, ApJ, 534, 870
 Smith et al. 2002, AJ, 123, 1502
 Smith et al. 2005, ApJ, 633, 392
 Takahashi & Portegies Zwart 2000, ApJ, 535, 759
 Yong et al. 2008, ApJ, 689, 1020

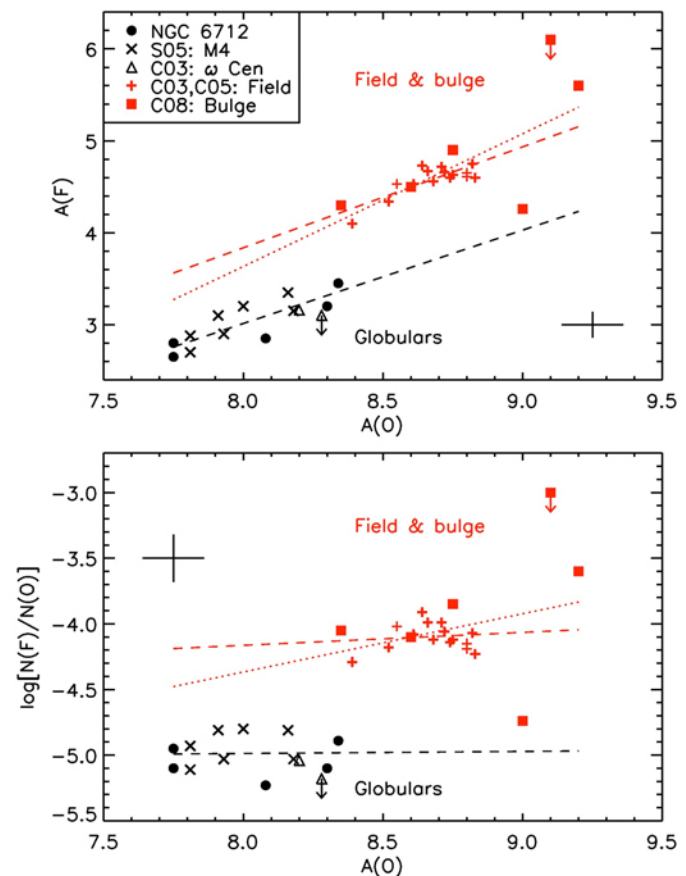


Figure 3: $A(F)$ vs. $A(O)$ (top) and $\log[N(F)/N(O)]$ vs. $A(O)$ (bottom). NGC 6712 (black circles), M4 (black crosses: Smith et al. 2005), ω Cen (black triangles: Cunha et al. 2003), bulge stars (red squares: Cunha et al. 2008), and field stars (red plus signs: Cunha et al. 2003; Cunha & Smith 2005) are shown. A representative error bar is shown. The red and black dashed lines are the linear least-squares fits to the field & bulge and globular cluster data, respectively (excluding upper limits). The dotted red line is the fit to the field & bulge data excluding the upper limits and the bulge star with $A(O) = 9.0$.

The Planetary Nebula View of M33: A Deep Spectroscopic Study with Hectospec

Laura Magrini (INAF), Letizia Stanghellini (NOAO) & Eva Villaver (STScI)

M³³ (NGC 598) is a spiral galaxy whose closeness (840 kpc, Freedman et al. 1991), optical size (53' × 83', Holmberg 1958), and inclination ($i = 53^\circ$) allow detailed studies of its stellar populations and ionized nebulae.

Planetary Nebulae (PNe) and HII regions represent two very different formation ages, and the comparison of these two populations provides insight to the chemical evolution of the host galaxy. Planetary nebulae are the final ejecta of evolved low- and intermediate-mass stars (LIMS) with masses between 1 and 8 M_\odot , which must have formed between 3×10^7 yr and 10 Gyr ago (Maraston 2005), while HII regions belong to a very young population.

During their evolution, LIMS do not modify the composition of the several elements that derive from the nucleosynthesis of Type II supernovae, such as oxygen, neon, argon, and sulfur—the so-called α -elements. Nucleosynthetic activity involving α -elements has been observed only in the lowest metallicity environments (Leisy and Dennefeld 2006; Magrini et al. 2005; Kniazev et al. 2008); evolutionary models confirm that at the metallicity of M33 one does not expect LIMS either to produce or destroy the α -elements (Marigo 2001). Thus, the observation of α -elements in PNe allows a measurement of the original metallicity of the interstellar cloud that gave birth to the LIMS.

On the other hand, the helium, nitrogen, and carbon abundances that we measure in PNe do not correspond to those at the time of the progenitor's formation, because these elements are synthesized in LIMS as well as in massive stars. These elements provide information about LIMS evolution as a function of their initial mass and metallicity, and, for a given metallicity, help to constrain the PN progenitor mass and age. The advantage of M33 compared to the Galaxy as a target for metallicity studies is that PNe in M33 have well-determined galactocentric distances, whose relative errors are <5%, much smaller than the large uncertainties of Galactic PNe distances (Stanghellini et al. 2008). In addition, the small inclination and the low reddening of M33 allow us to investigate the PNe population (and other stellar populations) across the whole radial range.

One of the most discussed issues in this field is the rate of evolution of the metallicity gradient in disk galaxies with time. Chemical evolution models predict different temporal behaviors of the metallicity gradient, depending on the assumptions one makes for gas inflow and outflow rates, and the star and cloud formation efficiencies. Observations are needed to constrain these assumptions, but so far they have been insufficient, especially for the old populations of PNe. Comparing different sets of results for the young and old stellar populations, such as HII regions and old stars, is also delicate, because the techniques of observing and analyzing nebulae and stars are very different, each with its own collection of uncertainties.

The motivation for our observations is to study the chemical and physical properties of a large number of PNe and HII regions in M33,

using the same observational procedures, the same data reduction and analysis techniques, and identical abundance determination methods, to avoid the biases due to the stellar versus nebular analysis. The aim was to derive abundances of the α -elements for as many PNe and HII regions as possible, and to study the variation of the metallicity gradients and the average abundances in M33 as compared with the Galaxy and other galaxies.

In semester 2007B, we observed ~150 ionized nebulae in M33 in multi-object spectroscopic mode with the MMT Hectospec fiber-fed spectrograph (Fabricant et al. 2005), with a 270 mm^{-1} grating at a dispersion of 1.2 \AA pixel^{-1} . The instrument deploys 300 fibers over a field of view 1° in diameter; the fiber diameter is 1" (4 pc using a distance of 840 kpc to M33). The 102 PNe were selected from the catalog by Ciardullo et al. (2004), and include four PNe at large galactocentric radii. We obtained spectra of 102 PNe and 48 HII regions with spectral coverage from ~3600 to 9100 \AA . The total exposure time was 4 hr, split into 8 sub-exposures of 1800 s each, taken on the nights of 13 October 2007 and 12 November 2007. The spectra were reduced and flux calibrated using the Hectospec package. The observed line fluxes, measured with the SPLOT package, were corrected for the effect of the interstellar extinction using the extinction law of Mathis (1990).

We used the extinction-corrected intensities to obtain the electron densities and temperatures of each PN with the commonly used diagnostic ratios: $[\text{S II}] \lambda\lambda 6716, 6731$ for the density, and $[\text{O III}] \lambda 4363 / (\lambda 5007 + \lambda 4959)$ and $[\text{N II}] \lambda 5755 / (\lambda 6548 + \lambda 6584)$ for the temperature. With the latter formulae we derive the electron temperatures of 34 PNe directly from our spectra; for the remaining PNe, we used the correlation between $I(\text{He II } \lambda 4686) / I(\text{H}\beta)$ and $T_e([\text{O III}])$, representing the effect of the central stars heating of the medium-high excitation nebulae. The ionic abundances were computed using the *nebular* analysis package in IRAF/STSDAS (Shaw & Dufour 1994). The elemental abundances were then determined by applying the ionization correction factors (ICFs) following the prescriptions by Kingsburgh & Barlow (1994) for the case where only optical lines are available.

Most of the PNe observed in M33 belong to its disk, while two PNe belong to the halo population (Ciardullo et al. 2004). We do not include the halo PNe in the following discussion. From the plot of N/O versus He/H, we found that there are 19 Type I PNe by Dopita's (1991) definition. Most PNe in our sample are non-Type I, implying a population mainly composed of PNe from old progenitors, with $M < 3M_\odot$, and ages > 0.3 Gyr.

We found a tight relationship between O/H and Ne/H in the M33 PNe (figure 1), thus broadly excluding modification of both elements during the lifetime of the progenitors, and validating the assumption that oxygen is a good tracer of the galaxy primordial metallicity. We also found that, generally speaking, the average elemental abundances of the α -elements in the M33 disk PNe are very similar to those of the Large Magellanic Cloud.

continued


Planetary Nebula View of M33 continued

In this preliminary paper we only present our PNe abundances; in order to assess the chemical evolution of M33, we used HII region observations from the literature (Rosolowsky & Simon 2008; Magrini et al. 2007a). The comparison between M33 PNe and HII region average abundances indicates a negligible global enrichment of the M33 disk from the epoch of the formation of the PNe progenitors to the present time.

The abundances of the α -elements were then used to compute the metallicity gradient of M33 by deriving the radial metallicity gradients of those elements that are not modified during the lifetime of LIMS—oxygen, neon, and sulfur. The element with the most reliable abundance, oxygen, has a slope of -0.031 ± 0.013 dex kpc^{-1} through the disk of M33 (figure 2). Within the errors, this slope is in agreement with the same gradient derived from the cumulative sample of HII regions described above, 0.032 ± 0.009 dex kpc^{-1} . Because the metallicity gradients of PNe and HII regions are practically indistinguishable from each other, and the mean abundances of the PNe and HII regions are very close, we conclude that the chemical enrichment in M33 from the time of the formation of the PN progenitors to the present time has been almost negligible.

A comparison of our results with chemical evolutionary models was done under the simplifying assumption that the age of all PNe is ~ 5 Gyr. The class of models that assume a halo collapse phase for the formation of the disk, such as Mollà et al. (1997), produce a PN gradient -0.025 dex kpc^{-1} steeper than the one for HII regions. Models assuming two infall episodes for the formations of the disk (first the thick disk, then the thin disk), such as Chiappini et al. (2001), predict PN gradients flatter than those of HII regions by about $+0.03$ dex kpc^{-1} . Finally, models assuming a slow formation of the disk from the intergalactic medium (Magrini et al. 2007b) predict a PN gradient -0.015 dex kpc^{-1} steeper than the one at the present time.

Our observations argue strongly that, within the errors, the slope of the metallicity gradients had small variations during the last several Gyr. Thus, our results exclude formation models of the disk of M33

that require rapid collapse scenarios and processes that produce changes in the metallicity gradients during the last Gyr. Rather, an extremely slow accretion from the intergalactic medium is favored for the formation of the M33 disk. Further, more detailed modeling is needed to confirm the formation scenarios of this disk galaxy. More details on this project can be found in Magrini et al (2008). 

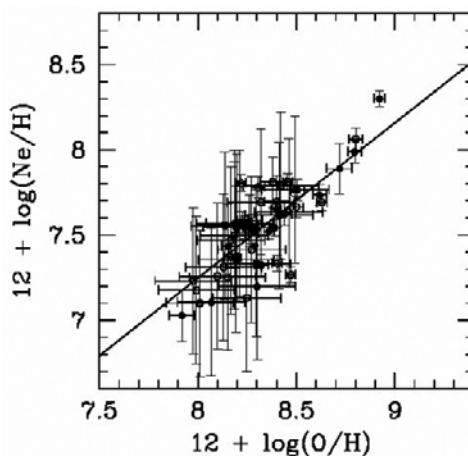


Figure 1: The relationship between oxygen and neon abundances. Filled circles refer to Type I PNe and empty circles to non-Type I PNe, following the definition of Dopita (1991). The continuous line is the weighted least-squares fit to the complete sample of PNe.

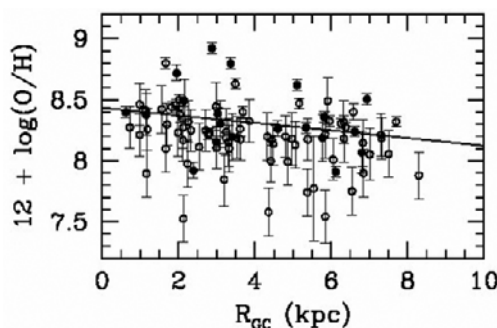


Figure 2: The radial gradient of oxygen abundance. Symbols are as in figure 1. The continuous line is the weighted least-squares fit to the complete sample of disk PNe.

REFERENCES

Ciardullo, R., et al. 2004, ApJ, 614, 167
 Chiappini, C., Matteucci, F., & Romano, D. 2001, ApJ, 554, 1044
 Dopita, M. A. 1991, IAUS, 148, 393
 Fabricant, D., et al. 2005, PASP, 117, 1411
 Freedman, W. L., Wilson, C. D., & Madore, B. F. 1991, ApJ, 372, 455
 Holmberg, E. 1958, Lund Medd. Astron. Obs. Ser. II, 136, 1
 Kingsburgh, R. L., & Barlow, M. J. 1994, MNRAS, 271, 257
 Kniazev, A. Y., et al. 2008, MNRAS, 388, 1667
 Leisy, P., & Dennefeld, M. 2006, A&A, 456, 451
 Magrini, L., et al. 2005, A&A, 443, 115
 Magrini, L., et al. 2007a, A&A, 470, 865
 Magrini, L., Corbelli, E., & Galli, D. 2007b, A&A, 470, 843
 Magrini, L., Stanghellini, L., & Villaver, E. 2008, ApJ, in press (arXiv:0901.2273v1)
 Maraston, C. 2005, MNRAS, 362, 799
 Marigo, P. 2001, A&A, 370, 194
 Mathis, J. S., 1990, ARA&A, 28, 37
 Mollà, M., Ferrini, F., & Diaz, A. I. 1997, ApJ, 475, 519
 Rosolowsky, E., & Simon, J. D. 2008, ApJ, 675, 1213
 Shaw, R. A., & Dufour, R. J. 1994, ASPC, 61, 327
 Stanghellini, L., Shaw, R. A., & Villaver, E. 2008, ApJ, 689, 194

A Candidate Sub-Parsec Supermassive Binary Black Hole System

Todd A. Boroson & Tod R. Lauer (NOAO)

A dramatic impact of the large survey archives now available, in particular, the Sloan Digital Sky Survey (SDSS), is that they have forced us to think about new ways to study large data sets. We need new techniques to learn what information is contained in a large set of observations, and we need new techniques to tease out the relationships that lead us to a physical understanding or to test our ideas. Large sets of spectra represent a particularly difficult problem, because different researchers will be interested in different kinds of information.

We have been applying an approach based on the Karhunen-Löeve Transform, or principal components analysis, to the spectra of the low-redshift, quasi-stellar objects (QSOs) in the SDSS archive to characterize the information contained in this data set. Our approach is based on the prescription of Connolly and Szalay (1999), who foresaw the capability of this technique to improve signal-to-noise ratios and fill in missing data in large, complex data sets. The procedure emphasizes the information in features that occur commonly in the ensemble of spectra and deemphasizes that which is in rare features, including noise. One of the consequences of this analysis is the identification of outliers, objects that are not well fit by the basis that describes the sample as a whole.

Having processed the 17,500 spectra of QSOs with $z < 0.7$ in the SDSS archive, we discovered a spectrum that seemed unique to us: a QSO with two broad-line systems. The spectrum of SDSS J153636.22+044127.0 (J1536+0441) is shown in the figure. This QSO has a g magnitude of 17.24 and 2MASS JHK magnitudes of 15.46, 14.85, and 14.10. It was detected by the Röntgen Satellite (ROSAT), but is not found in either the Faint Images of the Radio Sky at Twenty-cm (FIRST) or the NRAO VLA Sky Survey (NVSS) radio survey catalogs. Its appearance is stellar in the SDSS images.

The spectrum of J1536+0441 shows two broad-line emission systems and one system of narrow absorption lines. The highest redshift system, the r-system at $z = 0.3889$, shows broad Balmer lines ($H\alpha$, $H\beta$, and $H\gamma$) and the usual narrow lines ([O II], [O III], [Ne III], [Ne V]) seen in low-redshift QSO spectra. The lowest redshift system, the b-system at $z = 0.3727$, shows broad Balmer lines ($H\alpha$ through $H\delta$) and broad Fe II emission, seen most strongly around 3000 Å in the rest frame. The identification of the ultraviolet Fe II emission in the b-system is confirmed by cross-correlating the spectrum with a composite QSO spectrum (Vanden Berk et al. 2001). A strong, narrow absorption-line system, the a-system, is also present, including the Mg II doublet ($\lambda\lambda$ 2796, 2803), the Mg I λ 2852 line, the Ca II K line, and the Na D doublet. The redshift of this system is 0.38783, which, in the QSO rest frame, is 240 km s⁻¹ less than that of the r-system and 3300 km s⁻¹ greater than that of the b-system.

The b-system is a very unusual system in that it shows no narrow or forbidden-line emission. The [O III] 5007 line, typically the strongest such line, would fall just off the blue edge of the r-system [O III] 4959 line, a region that is otherwise quite clean. A conservative upper limit on the equivalent width of a line at this position is about 0.5 Å. This is about 2% of the measured strength of the r-system [O III] 5007 line. While there are a few QSOs known with no detectable [O III] lines, they are exclusively infrared-luminous objects that have extremely strong optical Fe II emission.

The interpretation of this object as a bound system of two black holes allows us to estimate the orbital parameters. The measured widths of the $H\beta$ lines are 2400 km s⁻¹ for the b-system and 6000 km s⁻¹ for the r-system. We apportion the luminosity at 5100 Å to the two black holes by assuming that the fraction attributable to each is proportional to its mass. This gives 10^{7.3} solar masses for the b-system black hole and 10^{8.9} solar masses for the r-system black hole. Alternatively, dividing the flux into equal halves would produce values of 10^{8.0} and 10^{8.8} for the two systems. If we then assume that we are observing this system at a random inclination and a random phase, we derive a separation of about 0.1 pc and an orbital period of about 100 years. Upper limits can be estimated from the assumption that we are seeing the system edge-on at a time when the relative velocity vector is in the line of sight. In that case, the separation is about 0.3 pc and the period is about 500 years.

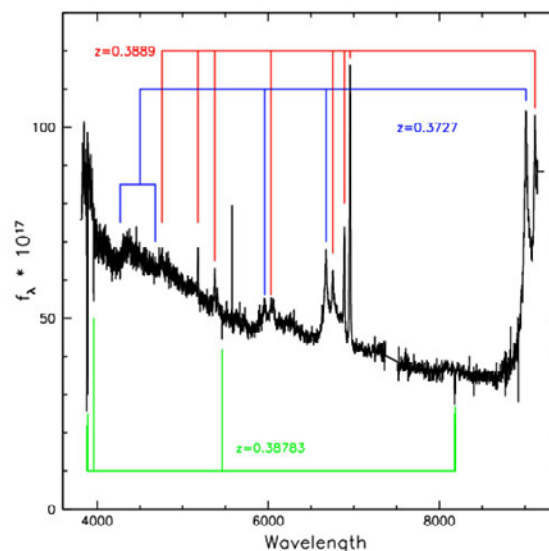
Of course, it is possible that the spectrum is the result of two objects that appear by chance in the same line of sight. We estimate the probability of this by integrating the SDSS QSO luminosity function (Rich-

ards et al. 2006) over a volume corresponding to a one-arcsecond radius circle and a depth that would put the object at a given redshift to within 10,000 km s⁻¹. This probability is 1.8×10^{-7} , which, when multiplied by the 17,500 objects in our sample, results in the expectation of 0.003 such objects. Although this is not negligible, we note the additional point of the unusual nature of the b-system spectrum as an argument that this is a single object with two black holes.

Future observations will determine the nature of this object. Better spectroscopy will allow better characterization of the two systems and perhaps detect associated starlight. High spatial resolution imaging may reveal the morphology of the host galaxy. Spectroscopic monitoring is critical, because our model predicts changes in the relative velocities as large as 150 km s⁻¹ in a single year. A paper on this object is in press in *Nature*.

REFERENCES

- Connolly, A. J., & Szalay, A. S. 1999, *AJ*, 117, 2052
 Richards, G. T., et al. 2006, *AJ*, 131, 2766
 Vanden Berk, D. E., et al. 2001, *AJ*, 122, 549



The observed spectrum from the SDSS archive of the QSO SDSS J153636.22+044127.0. The three redshift systems discussed in the text are indicated with most of the identified features marked. The strong unmarked emission feature is an artifact from poor subtraction of the night sky line at λ 5577.